Combining Wavelets and AR Identification for Condition Monitoring of Electric-cam Mechanisms Using PLCopen Readings of Motor Torque

Roberto Diversi[1], Nicolò Speciale[2], and Matteo Barbieri[3]

[1,2,3] *Department of Electrical, Electronic and Information Engineering, University of Bologna,*
Viale del Risorgimento 2, 40136 Bologna, Italy
roberto.diversi@unibo.it
nicolo.speciale@unibo.it
matteo.barbieri15@unibo.it

ABSTRACT

This paper addresses the problem of monitoring the state of health of electric motor driven mechanisms. The proposed condition monitoring procedure belongs to the data-driven methods and employs a combination of wavelet analysis and autoregressive model identification. It exploits the fact that the torque motor signal is a readily available measurement in industrial computers complying with the PLCopen standard and how motion controllers execute electric cams. In particular, the torque provided by the PLC is represented as the sum between the ideal torque and an additional contribution that contains information about mechanism health condition. The procedure completely removes the ideal torque and analyzes the residual component to highlight and classify possible fault conditions. The described condition monitoring procedure is tested on real data in a laboratory setup.

1. INTRODUCTION

Prognostics and Health Management (PHM) have significantly gained importance within the context of Industry 4.0, emerging as pivotal concepts in the research and development within the industrial automation sector (Gouriveau, Medjaher, & Zerhouni, 2016). In the realm of heavy-duty machinery, the occurrence of component failures is a common concern. Addressing the diagnosis of their health status and predicting their remaining useful life (RUL) has become a focal point of research efforts in the field (Soualhi et al., 2017; Qi, Zhang, & Spencer, 2023). This advancement owes much to the ever-increasing computational capabilities of computers, spanning from on-board processing (edge-computing) to external systems like industrial computers and cloud-based computing.

Condition Monitoring (CM) concerns the evaluation of the health status of equipment and components while they are actively engaged in machinery operations and tasks. Such notion is the founding element of any implementation of PHM. Indeed, research in this field primarily focuses on diagnosing and predicting faults that may arise in critical machine components, encompassing everything from bearings and gears to mechanical drive components and electrical systems (Lee et al., 2014). In particular, it's possible to categorize the main methods used in condition monitoring into three types, based on their mathematical utilization of physical knowledge related to the systems involved: model-based, data-driven, and hybrid methods (Gouriveau et al., 2016).

Firstly, Model-Based methods (Isermann, 2005) rely on physical modelling to build mathematical approximations of increasing degree of complexity to characterise systems' input/output behaviour. These methods run together with the machinery under monitoring to provide information on the internal state of the systems they represent. Physical modelling is particularly effective for the diagnosis and prognosis of faults. Its complexity may result prohibitive in terms of both the time required to define a model suitable for CM and the computational resources needed to run it on industrial computers or edge-computing microprocessors. Secondly, Data-Driven methods (Cerrada et al., 2018) exploit signals measured on-board the system to perform CM, mainly by means of signal processing and machine learning techniques. The implementation of such strategies is simpler and requires, in general, less time and resources. The information such methods extract can be effectively used to perform CM and then PHM on machinery even though it is typically of lesser quality than the model-based one. Finally, hybrid methods combine the previously mentioned ones.

Properly defined CM-based procedures require significant sensor measurements, suitable data processing algorithms and

appropriate servicing choices (either automated or with human intervention). Condition-Based Maintenance (CBM) and Predictive Maintenance (PM) encapsulate formally such concepts by defining a broader picture of the course of actions involved by dividing it into three macro-steps (Jardine, Lin, & Banjevic, 2006)

1. Data acquisition.
2. Data processing.
3. Maintenance decision-making.

In this work, we focus mostly on the first two steps, laying the groundwork for the third. The technique we exploit belongs to the data-driven methods and employs a combination of wavelets (Strang & Nguyen, 1996) and black box system identification theory (Söderström & Stoica, 1989): the first is widely used in CM, mainly as a feature extraction methods and filters, while the second consists in determining a parametric model (e.g. AR, ARMA) of the processed signals and to extract discriminative features from it (Isermann, 2006). We refer to the latter approach as Model-of-Signals, like in (Barbieri et al., 2018; Barbieri, Diversi, & Tilli, 2019).

On the one hand, wavelets are a versatile mathematical tool enabling the decomposition of complex signals and data into multiple scales, allowing for efficient analysis of both time and frequency domains simultaneously. They offer localized analysis, which means they can capture and localize transient events and variations in non-stationary signals. This property is particularly useful for CM purposes, since it allows to filter out unwanted components from signals. By considering discrete wavelets, such filtering can be easily implemented on industrial computers. On the other hand, Model-of-Signals relies on the signals measured and processed on-board the monitored machine to build dynamic models by means of system identification algorithms (Söderström & Stoica, 1989; Box, Jenkins, Reinsel, & Ljung, 2015). Models carry inherent information about the system physical content and the availability of recursive algorithms permits the implementation directly on the PLC, exploiting its edge-computing capabilities. Furthermore, Model-of-Signals methods compress signals information into models that are easier to handle. This allows the use of distributed computing frameworks with models becoming features for PHM algorithms.

This work presents a CM application where the combination of wavelets and Model-of-Signals aims at monitoring the state of health of electric motor driven mechanisms. In this context, the major part of the proposed CM procedures relies on vibration signals (Qi et al., 2023). An alternative consists in exploiting current motor signals (Nandi, Toliyat, & Li, 2005). The use of current measurements, that are related to the motor torque, was initially adopted only to monitor the internal health state of the motor (Nandi et al., 2005). Subsequently, the approach has been extended to the CM of the mechanism attached to the electric motor, leading to the so-

called motor current signature analysis (MCSA) method (Kar & Mohanty, 2006; Singh & Kumar, 2017; Chai, Yang, Ni, & Xu, 2018). The method proposed in this paper exploits the fact that the torque signal is a readily available measurement in industrial computers complying with the PLCopen standard (Foundation, 1992) and how motion controllers execute electric cams. Indeed, nowadays most industrial automation components manufactures comply with the standard, therefore the majority of motion controllers and PLCs with motion control allow for the implementation of our proposition. The described condition monitoring technique aims at providing the manufacturer with a PLC practicable solution for drive-mechanism fault detection.

The main idea is the following: the majority of electric cam motion tasks for servo drives are implemented as piece-wise polynomial trajectories with order lower or equal to 7. Therefore, in the case of linear mechanisms the ideal torque demanded by their motion is linked to the second derivative of such functions. In real applications, however, another component is present alongside the ideal torque: smaller with respect to the latter, but necessary to achieve the desired motion. Our conjecture on that additional contribution is that it contains information about the mechanism health condition and it can be modelled by a an Auto-Regressive (AR) model. Its analysis require the ideal contribution to be removed in order to prevent it from masking changes within the useful one (in this domain, the ideal torque is the "noise" perturbing the informative signal). A simple subtraction of the ideal torque could be arranged in this respect, however, it would depend on the given cam trajectory and on the equivalent inertia of the mechanism. In this work, we propose to filter out that ideal component using a particular property of a specific set of wavelet-based filters, exploiting the polynomial nature of the cam trajectory. Then, the useful part of the signal will be modelled as an AR process. This allows Model-of-Signals to be applied following its basic idea as in (Barbieri et al., 2018; Barbieri, Diversi, & Tilli, 2020; Barbieri, Nguyen, Diversi, Medjaher, & Tilli, 2021).

The remainder of the paper is organised as follows: Section 2 describes the torque model employed for condition monitoring. Section 3 concerns the extraction of the informative part of the torque signal through wavelet analysis. The proposed CM procedure is described in Section 4. In Section 5 we apply the proposed procedure to real data in a laboratory setup whose outcomes are shown in Section 6. Finally, conclusions are drawn in Section 7.

2. TORQUE MODELLING FOR CONDITION MONITORING

The majority of industrial machines rely on cams to perform complex tasks that require synchronisation among the various mechanisms involved. Cams can be divided into mechanical

and electrical. The use of the latter to perform synchronised operations is increasing in the last decades due to their comparable precision and greater flexibility with respect to mechanical ones. Electric cams allow to coordinate the motion of different mechanisms independently driven by electrical motors. This is possible because servo drives have become able to precisely track given position profiles commanded via Fieldbus by the motion controller, allowing the synchronisation of movements via software. Here, the most commonly used software library to program and command electric cams motion trajectories to servodrive is the PLCopen standard for motion control. Such library allows the implementation of motion control using the programming languages of the IEC 61131-3 standard. In particular, a vendor compliant with both standards has the built-in function *MC ReadActualTorque* to sample the motor applied torque during a motion command, providing a readily available signal to use for condition monitoring.

2.1. PLC implementation of electric cams

Electric cams are performed by linking together the trajectories of the different motors involved in the synchronised task: a leader, known as master, performs the guiding trajectory while one or more followers, called slaves, move accordingly. The coupling is established geometrically so that any given master trajectory point corresponds to a given slave trajectory point. This coupling is usually programmed by the user on the PLC vendor Integrated Development Environment (IDE). The typical implementations rely on the definition of via-points within the trajectory, which are then connected through mathematical functions which depend on the trajectory constraints. In most cases, polynomial functions, with their smoothness degree dependent on the number of constraints, are used. The constraints, in this case, originate from the required trajectory derivatives at those via-points. For instance, to build a master-slave synchronisation we need the master trajectory in position, $\vartheta(t)$ and the relative slave position evolution $q(\vartheta(t))$, denoted as $q(\vartheta)$ for simplicity. This definition allows to geometrically connect the two trajectories, while time enters indirectly with the master position, allowing speed variations without affecting synchronisation. Obviously, also the physical limits of the system affect the trajectory (e.g. the maximum allowed speed and acceleration) and have to be taken into account during the design phase. An example of synchronisation definition procedure is given as follows:

$$
\begin{aligned}
&q_1(0°) = 0°, && q_2(180°) = 360°, && q_3(360°) = 0°, \\
&\dot{q}_1(0°) = 0, && \dot{q}_2(180°) = 0, && \dot{q}_3(360°) = 0, \quad (1) \\
&\ddot{q}_1(0°) = 0°^{-1}, && \ddot{q}_2(180°) = 0°^{-1}, && \ddot{q}_3(360°) = 0°^{-1},
\end{aligned}
$$

where $q_i(\vartheta), \dot{q}_i(\vartheta), \ddot{q}_i(\vartheta)$ denote the position, speed and acceleration of the slave related to the i–th via-point. In this

case, q_1 is connected to q_2 with a polynomial function of order 5 since there is a total of 6 constraints. The same reasoning can be done for the cam piece between q_2 and q_3, with the final result shown in Fig.1. If we assume that master speed is constant, $\dot{\vartheta}(t) = const = \Omega_p$, then the x-axis can be directly translated in time by means of $t = \vartheta(t)/\Omega_p$. We refer to (Biagiotti & Melchiorri, 2008) for a complete discussion on how trajectories are generated.

2.2. The Torque Model

Suppose that the controller of the motors we want to synchronise is correctly designed and tuned. The master operates at constant speed followed by the slave with a trajectory defined as in (1) driving a linear mechanism. The torque required to perform the task in this case is

$$
\bar{T}(t) = J\ddot{\alpha}(t) = J\ddot{q}(t), \tag{2}
$$

where $J > 0$ is the moment of inertia and $\alpha(t) = q(\vartheta(t))$ is the angular position of the slave. If the number of via-points is M, $\bar{T}(t)$ is a piece-wise polynomial trajectory based on M couples of master-slave points and their constraints, with the former converted into their time counterparts $t \in [t_1 \ \dots \ t_M]$ following the constant speed assumption (see Subsection 2.1). Therefore, the torque trajectory segments correspond to the second derivative of the related position profile piece scaled by the inertia factor J. This can be formally described as follows:

$$
\bar{T}(t) = \begin{cases}
P_{n_1}^1(t) & t \in [t_1, t_2] \\
\vdots & \vdots \\
P_{n_k}^k(t) & t \in [t_k, t_{k+1}] \\
\vdots & \vdots \\
P_{n_{M-1}}^{M-1}(t) & t \in [t_{M-1}, t_M]
\end{cases} \tag{3}
$$

where

$$
P_{n_k}^k(t) = \gamma_0^k + \gamma_1^k t + \gamma_2^k t^2 + \cdots + \gamma_{n_k}^k t^{n_k} \tag{4}
$$

is the polynomial piece corresponding to the time interval $[t_k, t_{k+1}]$, with coefficients $\gamma_i^k, i = 1, \dots, n_k$, $n_k = d_k - 2$ is the polynomial degree and d_k is the degree of the polynomial of the respective trajectory position.

As previously mentioned, the torque measurement from the slave axis is readily available in PLCs implementing electrical cams. Indeed, motor applied torque can be sampled using the PLCopen function *MC ReadActualTorque* in the majority of motion control enabled industrial controllers. This signal carries the ideal torque profile required by the mechanism, as in (2), together with parametric uncertainties in J in addiction to unmodelled ones (e.g friction, control adjustments and induced vibrations). As stated in Section 1, our conjecture is that the information about the machine state of health is con-
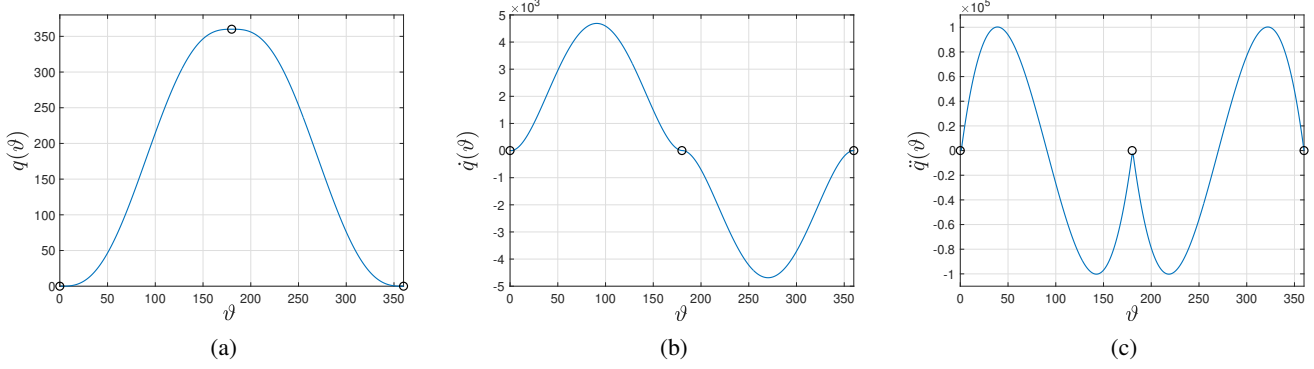
Figure 1. Example of piece-wise polynomial cam: (a) Position; (b) Speed; (c) Acceleration. Via-points are denoted by circles, master and slave positions are in degrees $[deg]$, while the acceleration is in $[deg^{-1}]$.

tained in this unknown part. If we are able to take out the ideal cam contribution, the remaining signal can then be used in the Model-of-Signals fashion to perform diagnosis. Based on these considerations, we propose to model the real torque signal provided by the PLC as follows

$$T(t) = \bar{T}(t) + e(t), \tag{5}$$

where $\bar{T}(t)$ is the ideal torque (3) and $e(t)$ is the remaining part of the signal, which is assumed to be representative of the health state of the system. The informative part of the signal $e(t)$ is modelled as an autoregressive (AR) process of order p:

$$e(t) + a_1\, e(t-1) + \cdots + a_p\, e(t-p) = w(t), \tag{6}$$

where $w(t)$ is a zero mean driving white noise process with variance σ_w^2. Model (6) can be rewritten in the form

$$e(t) = \frac{w(t)}{A(z^{-1})} \tag{7}$$

where $A(z^{-1}) = 1 + a_1\, z^{-1} + \cdots + a_p\, z^{-p}$ is a polynomial in the unit delay operator z^{-1}, i.e.$z^{-1}e(t) = e(t-1)$. The AR process $e(t)$ can thus be seen as the output of an all-pole filter driven by a white process. Model (6) can be rewritten in the regression form

$$e(t) = \varphi^T(t)\theta + w(t) \tag{8}$$

where

$$\varphi(t) = \left[\, -e(t-1)\ -e(t-2)\, \cdots\, -e(t-p)\, \right]^T \tag{9}$$

$$\theta = \left[\, a_1\ a_2\ \cdots\ a_p \,\right]^T. \tag{10}$$

Following these reasonings, the main steps of the proposed procedure for condition monitoring can be summarized as follows:

1. Remove from the measured torque $T(t)$ the piece-wise polynomial part $\bar{T}(t)$, in order to extract the informative part $e(t)$.

2. Identify an autoregressive model of the signal $e(t)$.

3. Extract, from the estimated AR model, the features for condition monitoring and compute an healthy indicator.

3. ESTIMATION OF THE INFORMATIVE SIGNAL WITH WAVELET ANALYSIS

The use of wavelets for condition monitoring of electric motor driven mechanisms is widely reported (Peng & Chu, 2004; Yan, Gao, & Chen, 2014; Soualhi et al., 2018), especially to improve the signal-to-noise ratio or to demodulate frequency bands for diagnosis from the envelope of the spectrum.

In this Section we describe a completely different use of wavelet analysis in order to extract the informative part of the torque signal provided by the PLC. It exploits both the advantages of multiresolution analysis theory and the vanishing moments property of the wavelet functions (Mallat, 1989; Daubechies, 1992).

3.1. Multiresolution representation of a signal

A multiresolution analysis $\{V_k\}_{k\in\mathbb{Z}}$ consists in a nested sequence of closed subspaces of $\mathbb{L}^2(\mathbb{R})$

$$\{0\} \subset \cdots \subset V_{k-1} \subset V_k \subset V_{k+1} \cdots \subset \mathbb{L}^2(\mathbb{R}).$$

For each scale k, all spaces must satisfy the property

$$s(t) \in V_k \Leftrightarrow s(2t) \in V_{k+1}$$

which ensures that signals in a space are simply scaled versions of those in the next one. Moreover, by introducing the space W_k as the orthogonal complement of V_k in V_{k+1}, it results

$$V_{k+1} = V_k \oplus W_k$$

An orthonormal wavelet system $\{\varphi_{k,n}, \psi_{k,n}\}_{k,n\in\mathbb{Z}}$ involves an infinite collection of integer translated and dyadic scaled versions of orthonormal scaling and wavelet functions respec-

tively:

$$\varphi_{k,n}(t) = 2^{k/2}\varphi(2^k t - n) \quad k,n \in \mathbb{Z}$$
$$\psi_{k,n}(t) = 2^{k/2}\psi(2^k t - n) \quad k,n \in \mathbb{Z}$$

According to the theory, V_k is spanned by $\{\varphi_{k,n}\}_{k,n \in \mathbb{Z}}$, W_k is spanned by $\{\psi_{k,n}\}_{k,n \in \mathbb{Z}}$ and for $s(t) \in \mathbb{L}^2(\mathbb{R})$

$$s(t) = \sum_{n \in \mathbb{Z}} c_{k_0,n}\varphi_{k_0,n}(t) + \sum_{k=k_0}^{\infty} \sum_{n \in \mathbb{Z}} d_{k,n}\psi_{k,n}(t)$$

being k_0 the coarsest scale (Mallat, 1989).

In real life situations where only the samples of a signal are known, there exists a highest possible resolution. By selecting $k_0 + 1$ as the sampling scale (with sampling rate of 2^{k_0+1} per unit interval), there exists a highest resolution when the finest scale is the sampling level. The signal can then be represented counting from $k = k_0$ down to some $k_1 < k_0$ as

$$s(t) = \sum_{n \in \mathbb{Z}} c_{k_1,n}\varphi_{k_1,n}(t) + \sum_{k=k_1}^{k_0} \sum_{n \in \mathbb{Z}} d_{k,n}\psi_{k,n}(t)$$
$$= s_{k_1}(t) + \sum_{k=k_1}^{k_0} d_k(t) \tag{11}$$

The first term $s_{k_1}(t)$ (*approximation*) is the projection of $s(t)$ onto the coarse space V_{k_1} spanned by $\varphi_{k_1,n}(t)$, and the second one provides the high resolution information $d_k(t)$ (*details*) spanned by the wavelet functions. This representation shows the signal components at each considered scale. The coefficients $c_{k_1,n} = \langle s, \varphi_{k_1,n} \rangle$ and $d_{k,n} = \langle s, \psi_{k,n} \rangle$ represent the Discrete Wavelet Transform (DWT). They completely describe the original signal and can be used in a way similar to Fourier series coefficients for analysis, approximation and filtering. Within the framework of the multiresolution analysis, to perform the DWT, one need just very simple digital filters. Indeed, both the scaling and the wavelet functions are solution of the two-scale difference equations

$$\varphi(t) = \sqrt{2} \sum_{n \in \mathbb{Z}} h_0[n]\varphi(2t - n) \tag{12}$$

$$\psi(t) = \sqrt{2} \sum_{n \in \mathbb{Z}} h_1[n]\varphi(2t - n) \tag{13}$$

where $h_1[n] = (-1)^n h_0[1-n]$ and the sequences $\{h_0[n]\}_{n \in \mathbb{Z}}$ and $\{h_1[n]\}_{n \in \mathbb{Z}}$ can be interpreted as the impulse response of a digital low-pass scaling filter $H_0(z)$ and a high-pass wavelet filter $H_1(z)$, having the same cutoff frequency. This fact leads to an efficient discrete-time algorithm based on a filter bank implementation to compute $c_{k_1,n}$ and $d_{k,n}$, making (11) useful in practice.

As shown in Figure 2, the process of decomposing a signal into approximation and details is realized as a low-pass

$H_0(z)$ and high-pass $H_1(z)$ filtering followed by a dyadic down-sampling (Mallat's multilevel algorithm). For a signal of length L, the maximum number of DWT levels is $\log_2 L$ at most. The process of analysis can be reversed by up-sampling by 2 and filtering with reconstruction filters derived from $h_0[n]$ and $h_1[n]$.

The design of the filter $\{h_0[n]\}_{n \in \mathbb{Z}}$ allows for the construction of wavelet systems with desirable properties (Daubechies, 1992). For example, it is possible to construct FIR filters that define compactly supported wavelets and scaling functions having space and frequency localization and vanishing moment property. With regard to the latter, a wavelet ψ has N vanishing moments when

$$\int t^l \psi(t)dt = 0 \qquad \text{for } l = 0, 1, 2\ldots, N-1 \tag{14}$$

or, equivalently, with the constraint on the low-pass filter:

$$\sum_n (-1)^n n^l h_0[n] = 0 \quad \text{for } l = 0, 1, 2\ldots, N-1 \tag{15}$$

Requiring the moments of the wavelet to be zero has several interesting consequences. In particular, all polynomials of degree up to $(N-1)$ can be express as a linear combination of $\{\varphi_{k_0,n}\}_{n \in \mathbb{Z}}$ (Strang & Nguyen, 1996), since, as shown by (14), the wavelet can correlate with the polynomial obtaining zero correlation coefficients. This observation is at the heart of the proposed approach.

3.2. Simulation example

To illustrate the use of the vanishing moments property, let us consider in Figure 3a a simple test signal $s(t) = P_3(t) + e(t)$ where $P_3(t)$ is a third-degree polynomial and $e(t)$ an AR signal of order $p = 6$. In the following, we use the Daubechies wavelet family dbN with $N = 4$. If the signal is described as in (11), the analysis with a wavelet having a sufficient number of vanishing moments with respect to the degree of the polynomial will produce a good approximation $\widetilde{P}_3(t)$ of $P_3(t)$ which we can get rid of by difference. Figure 3b shows the reconstructed AR process $\hat{e}(t) = s(t) - \widetilde{P}_3(t)$.

To test the accuracy of the estimated AR signal $\hat{e}(t)$ an identification experiment has been performed. First, starting from the estimated signal $\hat{e}(t)$ of Figure 3b the order of suitable AR model has been estimated by means of the minimum description length (MDL) criterion (Ljung, 1999). The results, described in Figure 3c, clearly indicate $p = 6$ as the correct order (the MDL function attains its minimum at $p = 6$). Subsequently, two AR models of order 6 have been identified by using the least squares method (Ljung, 1999) from the true AR signal $e(t)$ and its reconstruction $\hat{e}(t)$ respectively. Figure 3d reports the poles identified from $e(t)$ and $\hat{e}(t)$. This confirms that the proposed method leads to an excellent reconstruction of the stochastic part $e(t)$.
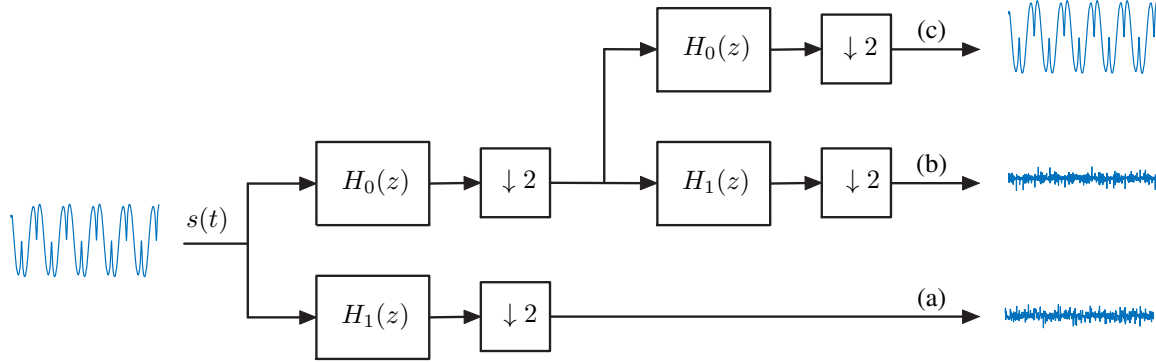
Figure 2. Two-channel filter bank implementation of the DWT algorithm. (a) and (b) are the details $d_k(t)$ at level 1 and 2 respectively; (c) is the approximation $s_{k_1}(t)$ at level $k_1 = 2$. The details have been magnified by a factor of 10 to make them visible.
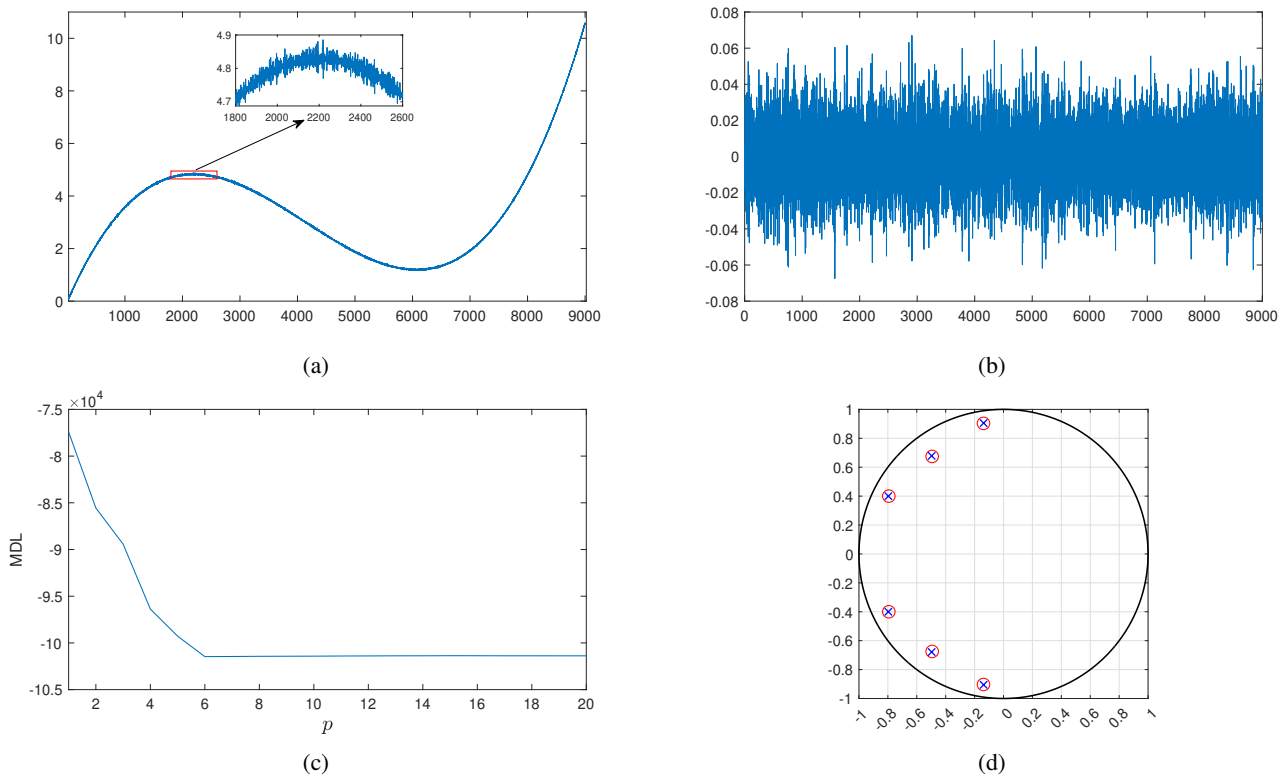
Figure 3. Simulation example. i) Extraction of the stochastic AR signal through $db4$ wavelet: (a) original polynomial signal with additive AR process; (b) reconstructed AR signal. ii) Identification of the AR model from the signal estimated through $db4$ wavelet. (c) Estimation of the AR order p with the MDL criterion ; (d) Comparison of the AR poles identified from the true AR signal (o) and from the reconstructed AR signal (x).

4. CONDITION MONITORING PROCEDURE

Following the reasoning in Section 2, the torque signal provided by the PLC is modeled as the sum of a cam nominal torque and an AR process containing information about the system so its difference with the approximation obtained by filtering with a suitable wavelet at scale k_e can get rid of it returning the stochastic part.

In our approach, the condition monitoring procedure can be divided into two distinct phases depicted in Figure 4 and Figure 5 respectively: parameters setting and online monitoring.

4.1. Parameters setting

Figure 4 shows the flow chart of the different steps required to obtain the main parameters used in the online monitoring phase.

By operating on a set of data $T_0(t)$ acquired under normal operating conditions ("Healthy case"), the wavelet type to use and at which scale to operate are selected. Among the many solutions in literature, we will focus on two-channel, compactly supported, and real-valued wavelet systems, the most fundamental and widely used in DSP applications. In particular, Daubechies wavelets dbN are optimal in the sense that they have the minimum support of size $2N - 1$ with the largest possible number N of vanishing moments. The finite support implies a finite number of coefficients in (12) and (13) i.e. $H_0(z)$ and $H_1(z)$ are FIR filters (Daubechies, 1992). Although in the following only this wavelet system is considered, other different families of functions that meet the vanishing moments property (14) can be considered as well.

Based on the known orders n_k of the polynomials in the ideal torque model (3), it is possible to choose the most suitable wavelet to be used for processing with $N \geq \max\{n_k\}$. Hence, the choice of a wavelet function is a trade-off between N and its support. In an ideal situation similar to the example described in Section 3.2, choosing the wavelet dbN with $N = n_k$ would require the use of only one analysis level $k_e = 1$. However, real cases are more complex. In order to perform detection and isolation, we determine the number k_e of analysis levels to be performed (i.e. the number of steps in the Mallat's algorithm) by considering an appropriate indicator of signal regularity. As well known, the behavior of a time series is the more predictable the greater the presence of repetitive patterns (periodicity). Due to (14), wavelet processing deletes the strongly regular polynomial component of the torque signal, producing a sequence in which almost exclusively random components are present: since entropy quantifies the amount of information, it also measures the degree of randomness in the system. To measure the non-predictability of the time series trend, among the entropy functions available, the Approximate Entropy (ApEn) (Pincus, 1995) was chosen. By doing so, a time series with many repetitive pat-

Table 1. Comparison of ApEn performance results for different type of Daubechies wavelets dbN and analysis levels k_e. For $k_e = 0$ no processing has been done: the ApEn low value of is due to the strong regular periodic component in the torque signal.

k_e	db2	db3	db4	db5	db6
0			0.1000		
1	1.3407	1.2716	1.3671	1.3627	1.3287
2	1.0488	1.1280	1.3592	1.2406	1.2801
3	0.7329	0.7257	0.7536	0.7192	0.7146
4	0.5992	0.4063	0.4190	0.4179	0.4466

terns produces a relatively small value of ApEn, while a less predictable process has a higher value of ApEn.

Therefore, in real cases the presence of non-idealities can be managed either by investigating several wavelets of the same family with slightly different values of N or considering $k_e > 1$ by performing at most one or two successive analyses. In this work, we have identified as a good criterion for choosing the k_e level the value that immediately precedes a significant decrease of ApEn. Examples of ApEn performance results depending on the type of Daubechies wavelets and different levels of analysis are shown in Table 1. By setting $k_0 = 0$ and $k_1 = -k_e$, the first term in (11) will represent a good approximation of $\bar{T}(t)$ with which to estimate the AR signal $\hat{e}(t)$ by difference.

At this point, an AR model of type (6)-(10) can be identified and reference features obtained for the next step. First, a suitable model order p is selected by means of some model order criteria like FPE, AIC, MDL (Ljung, 1999). They consist in selecting the order p as follows

$$FPE: \quad p = \min_i \left(\frac{L+p}{L-p} J(\hat{\theta}^i) \right) \tag{16}$$

$$AIC: \quad p = \min_i \left(L \log J(\hat{\theta}^i) + 2\,i \right) \tag{17}$$

$$MDL: \quad p = \min_i \left(L \log J(\hat{\theta}^i) + i \log L \right) \tag{18}$$

where L is the number of available samples of $\hat{e}(t)$, $J(\hat{\theta}^i)$ is the least squares loss function

$$J(\hat{\theta}^i) = \frac{1}{L-i} \sum_{t=i+1}^{L} (\hat{e}(t) - \varphi^T(t)\hat{\theta}^i)^2 \tag{19}$$

and $\hat{\theta}^i$ is the least squares estimate of an i–th order AR model:

$$\hat{\theta}^i = \frac{1}{L-i} \left(\sum_{t=i+1}^{L} \varphi(t)\varphi^T(t) \right)^{-1} \frac{1}{L-i} \sum_{t=i+1}^{L} \varphi(t)\hat{e}(t). \tag{20}$$
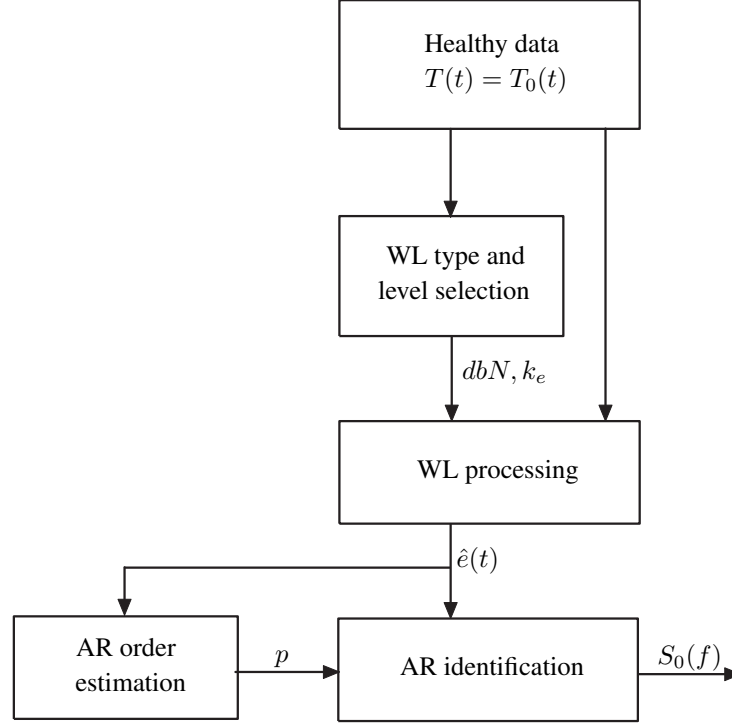
Figure 4. Flowchart of the parameters setting phase. The starting point is a set of L samples of the PLC torque $T_0(1), T_0(2), \ldots, T_0(L)$, collected under normal (healthy) operating conditions. The Daubechies wavelet dbN and the number of wavelet analysis levels k_e are selected. Then, the informative signal $\hat{e}(t)$ is estimated. On the basis of $\hat{e}(t)$, the AR model order p is selected and the nominal p-order AR model is identified. Finally, the associated PSD $S_0(f)$ is computed.

Once that the order p is estimated, the nominal (reference) model $\hat{\theta}_0$ is obtained by evaluating (20) for $i = p$: $\hat{\theta}_0 = \hat{\theta}^p$. The feature that will be exploited for condition monitoring is the power spectral density (PSD) of the identified AR model, given by (Box et al., 2015)

$$S_0(f) = \frac{\hat{\sigma}_{w0}^2}{|\hat{A}_0(e^{-j2\pi f})|^2} = \frac{\hat{\sigma}_{w0}^2}{|1 + \sum_{k=1}^{p} \hat{a}_{k0}\, e^{-j2k\pi f}|^2} \tag{21}$$

where $\hat{a}_{10} \ldots, \hat{a}_{p0}$ are the entries of the estimated vector $\hat{\theta}_0$ and $\hat{\sigma}_{w0}^2 = J(\hat{\theta}_0)$.

4.2. Online monitoring

Figure 5 shows the main steps of the proposed condition monitoring method. They can be summarized as follows:

1. Preprocessing of the PLC torque signal $T(t)$ (buffering and windowing)

2. Wavelet analysis (MRA representation) to obtain the estimation $\hat{e}(t)$ of the informative part of the torque signal;

3. Identification of an AR model of $\hat{e}(t)$ and determination of the associated PSD $S(f)$;

4. Generation of the healthy indicator by comparing $S(f)$ with the nominal PSD $S_0(f)$.

In the first step, the real-time signal $T(t)$ is divided in buffered and windowed sequences of L samples to improve the results of the processing. Since the buffered signal has a finite length, artificial discontinuities are introduced at its edges, which, if not handled correctly, can damage subsequent analysis steps. In the second step, a wavelet analysis at the k_e scale with the chosen $\psi(t)$ function is performed. By doing so, the k_e-level approximation $\tilde{T}(t)$ of the periodic component of the torque is subtracted from the data to obtain the AR signal $\hat{e}(t)$. In the third step, a p–order AR model $\hat{\theta}$ of the extracted signal $\hat{e}(t)$ is estimated by means of the least squares method, see (20). The variance $\hat{\sigma}_w^2 = J(\hat{\theta})$ is also estimated. From $\hat{\theta}$ and $\hat{\sigma}_w^2$ the power spectral density $S(f)$ is computed, see (21). In the last step, the healthy indicator is obtained by comparing the current PSD $S(f)$ with the nominal one $S_0(f)$. In particular, we propose to use the Symmetric Itakura-Saito Spectral Distance (SISSD), also called COSH distance (Wei & Gibson, 2000):

$$SISSD = \frac{1}{N_f} \sum_{k=1}^{N_f} \left(\frac{S_0(f_k)}{S(f_k)} - \log \frac{S_0(f_k)}{S(f_k)} \right.$$
$$\left. + \frac{S(f_k)}{S_0(f_k)} - \log \frac{S(f_k)}{S_0(f_k)} - 2 \right) \tag{22}$$
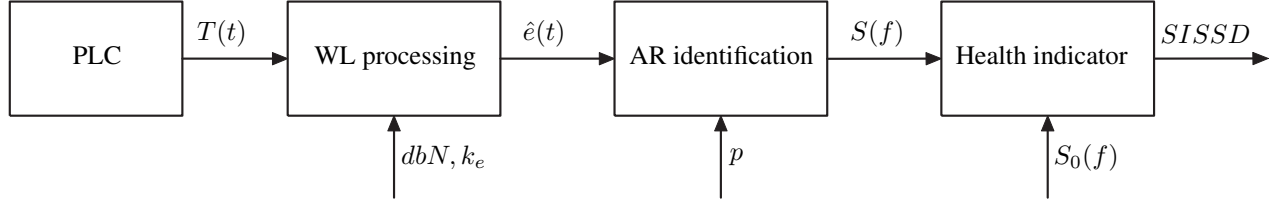
Figure 5. Flowchart of the online monitoring procedure. After buffering and windowing, a wavelet processing is performed on the measured torque signal $T(t)$ to extract the informative signal $\hat{e}(t)$. AR identification is then performed to estimate the AR parameters and the corresponding PSD $S(f)$. Finally, the healthy indicator $SISSD$ is computed by comparing the current PSD $S(f)$ with the reference one $S_0(f)$. The quantities dbN, k_e, p and $S_0(f)$ are fixed as they are computed during the parameters setting phase.

where N_f is the number of frequencies considered in the evaluation of the power spectral densities. It is worthwhile noting that spectral distances have to be preferred w.r.t the euclidean distance $\|\hat{\theta} - \hat{\theta}_0\|^2$ when AR models are exploited in detecting signal changes (Basseville, 1988). Moreover, in the Gaussian case, the Itakura-Saito distance corresponds to the Kullback-Leibler divergence up to a multiplicative factor (Grivel, Diversi, & Merchan, 2021) so that it has also a statistical interpretation.

By exploiting the multiresolution representation and the wavelet zero moment property, the proposed approach allows both real-time analysis and no invasive procedure in standard industrial set-up since it is based on an efficient digital filtering of a signal normally available in PLCs. Similar considerations can also be made for the identification of AR models of the extracted informative signals. For instance, the LS estimate (20) can be computed by means of the recursive least squares algorithm (Söderström & Stoica, 1989), whose computational efficiency allows an easy implementation on a PLC (Barbieri et al., 2018, 2021).

5. CASE STUDY

5.1. Experimental setup

The experimental setup utilised is presented in Fig. 6 and is composed by: electrical motor (1), rigid joint (2), shaft and flywheel with two half-moon shaped weights (3). The cabled encoder (4) in the figure is not used in this experimental analysis and is not taken into account. The inertia of the system can be divided into two parts: one is fixed, with a value of $J_{fix} = 0.0015[kg/m^2]$, and one is variable $J_w = J_{w_1} + J_{w_2}$ depending on the two attached weights, J_{w_1} and J_{w_2}. The mechanism is driven by B&R equipment: the PLC is the *Automation PC 910* connected to an *ACOPOS P3* servo drive controlling a brushless motor *8LSA36DB030S000-3*. The electric cam utilised is the same as in (1) (see also Fig. 1) performed using a virtual master running at constant speed $\Omega_p = 1080°/s$. The synchronised motion task time was chosen to be $T_s = 0.0008s$ since the system only allows time-steps of $0.0004s$ or multiples and that was the recommended setting.

Therefore, the measurement of the torque signal has the same resolution and is collected by means of the tracing system provided by B&R IDE, Automation Studio, with a sampling frequency of $1250Hz$ and can be directly saved into .mat format. To test the proposed monitoring approach we sampled the slave drive torque during the synchronised motion of the system with both symmetric and asymmetric (i.e unbalanced) load. The former being the healthy reference operating point and the latter being the faulty one achieved by modifying one of the two half-moon shaped weights with a slightly thicker and a slightly thinner one. In addition, in the symmetrical case, one of the two weights has been loosened by sightly unfastening the bolts that keeps it in place to simulate a fault with increased degree of severity. Those unbalanced loads should generate changes in the informative part of the torque measurement which in turn should be captured by the models. The four tested configurations are reported below:

Config. (1) Symmetric load:

$$J_{w_1} = 7.1305 \cdot 10^{-4}, \ J_{w_2} = 7.1305 \cdot 10^{-4}[kg/m^2] \tag{23}$$

Config. (2) Asymmetric increased load:

$$J_{w_1} = 7.1305 \cdot 10^{-4}, \ J_{w_2} = 7.5030 \cdot 10^{-4}[kg/m^2] \tag{24}$$

Config. (3) Asymmetric decreased load:

$$J_{w_1} = 7.1305 \cdot 10^{-4}, \ J_{w_2} = 6.1725 \cdot 10^{-4}[kg/m^2] \tag{25}$$

Config. (4) Loose Symmetric load: same as Config. (1) but with loosened bolts in one of the weights:

$$J_{w_1} = 7.1305 \cdot 10^{-4}, \ J_{w_2} = 7.1305 \cdot 10^{-4}[kg/m^2]$$
$$\text{(loosened bolts)} \tag{26}$$

Various measurements of the slave torque were collected during operations in all configurations. Then, they were processed by simulating a PLC implementation via Matlab according to the procedures summarized in Figs. 4 and 5 for the parameters setting and the online monitoring respectively.

9
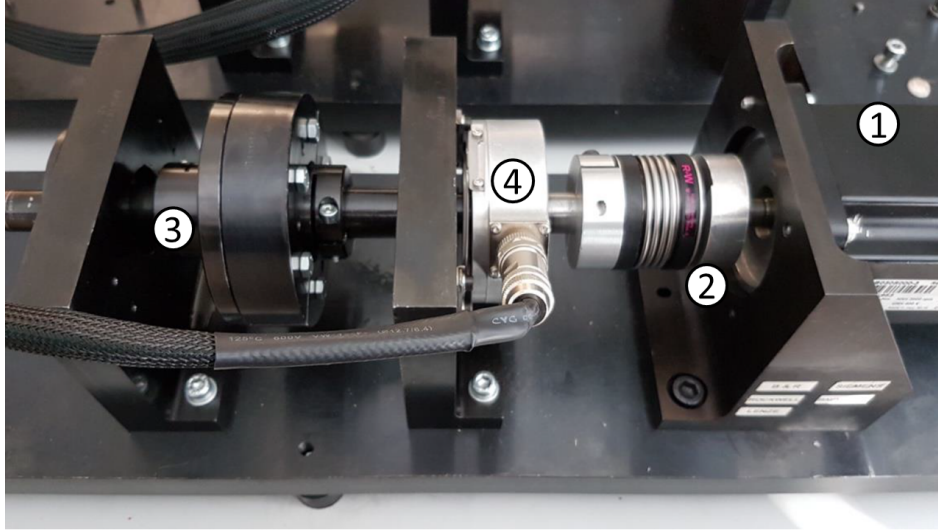
Figure 6. Experimental linear rigid mechanism setup. Variable weights are attached to the flywheel (number 3) on the left side of the shaft using bolts.

The buffer and process architecture is applicable to any PLC since it allows the storage of L data samples to be coded within the main priority task, in this case with a sampling time of $T_s = 0.0008s$, and the implementation of their processing in a secondary task of lower priority, without affecting significantly the system memory and the control program computational load. This keeps the condition monitoring task on-line, still able to check machine health state with respect to degrading faults. For instance, the procedure summarized in Fig. 5 can be performed every few seconds while mechanism degradation due to friction or wearing or heat typically takes minutes to hours to even days.

5.2. Experimental results

The torque measurements collected during the experiment in the four tested configurations (23)–(26) are divided into sequences of length $L = 5000$ samples, corresponding to 4 seconds. The first ten sequences of Configuration (1) (symmetric load) have been used to perform the parameters setting phase summarized in Fig. 4 since this configuration can be considered as the healthy condition of the mechanism. According to the procedure described in Subsection 4.1 the Daubechies wavelets $db4$ with $k_e = 2$ analysis levels was first selected. Then, for each of the ten healthy sequences, the corresponding informative signal $\hat{e}(t)$ was extracted. The model selection criteria (16)–(18) were applied on the ten informative signals to determine a suitable order for the AR models. The most clear indication was obtained with the MDL criterion, that exhibits a minimum around the order 50 in all sequences. The AR order $p = 46$ was finally selected. The reference AR model $\hat{\theta}_0$ is computed as the mean of the ten AR models of order 46 identified from the informative signals and the

associated reference PSD $S_0(f)$ was computed, see (21).

The online monitoring phase was performed on the rest of the healthy sequences (Configuration (1)) and on all the faulty sequences related to Configurations (2), (3) and (4) according to the procedure described in Subsection 4.2 and summarized in Fig. 5. This means that every torque sequence of length $L = 5000$ leads to a value of the healthy indicator $SISSD$ computed from (22). Figure 7 shows a sequence of the measured torque $T(t)$ for each of the four conditions (23)–(26) and the corresponding informative part $\hat{e}(t)$ obtained through the wavelet analysis. Figure 8a reports the evolution of the healthy indicator $SISDD$ in the four configurations (23)–(26) while Fig. 8b is a zoom that better highlights the behaviour of $SISSD$ in the first three conditions. Figure 9 compares the nominal PSD $S_0(f)$ obtained in the parameters setting phase with one the PSDs $S(f)$ obtained in the four configurations (23)–(26) during online condition monitoring. It is evident that the condition monitoring task is carried out successfully. In healthy conditions (Configuration (1)) the $SISSD$ is close to zero (see Fig. 8a) as the current PSD is quite close to the reference one, see. Fig. 9a as an example. In all faulty conditions, the mean value of the $SISSD$ increases by a factor of at least 5 w.r.t the healthy condition, as shown in Fig. 8 and Table 2. A robust fault detection is thus obtained as the healthy status (1) can be clearly distinguished from the faulty conditions (2), (3) and (4). It is worth noting that the adopted scalar indicator allows also to perform the fault isolation task. In fact, it is clear from Fig. 8 that it is possible to set robust thresholds that allow to distinguish each condition from the others.

To show the influence of signal windowing on the whole procedure, both the parameters setting and the online monitoring
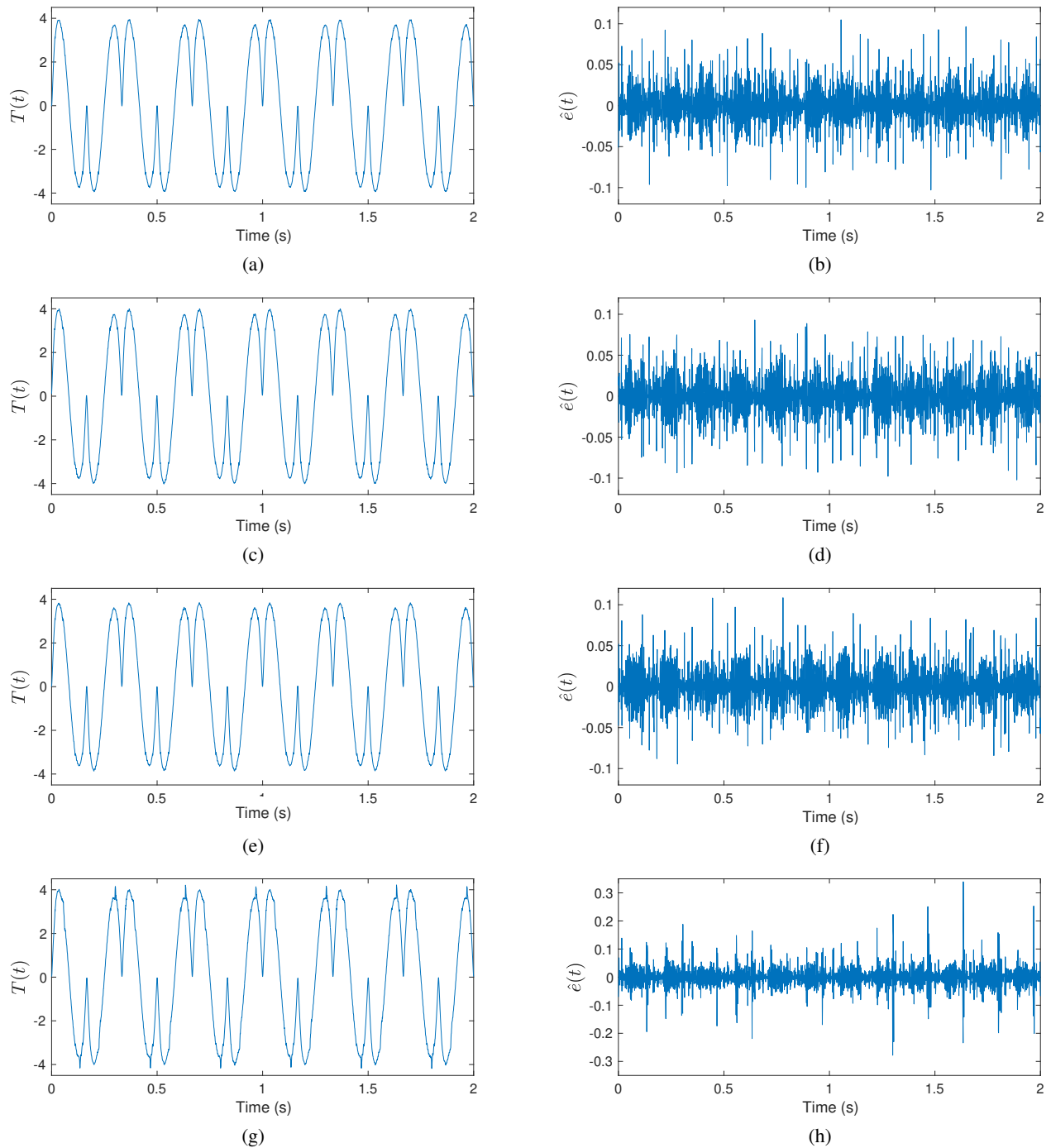
Figure 7. Real torque signals and corresponding informative parts extracted through Daubechies $db4$ wavelet in different conditions: (a)(b) symmetric load (healthy state); (c)(d) asymmetric increased load; (e)(f) asymmetric decreased load; (g)(h) loose symmetric load. For the sake of readability only the first 2 seconds (2500 samples) are shown.

(a)

(b)
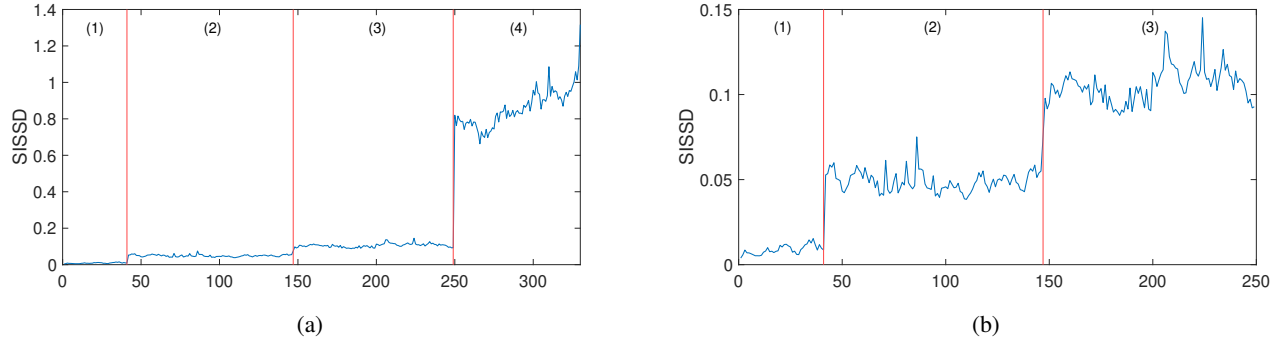
Figure 8. Evolution of the healthy indicator $SISSD$ in the different conditions (23)–(26). Each value of the $SISSD$ has been obtained starting from a sequence of length $L = 5000$, a $db4$ wavelet analysis and an AR model of order $p = 46$. (a) all configurations are considered; (b) zoom of (a) to clearly show the behaviour of the $SISSD$ in the first three conditions.

(a)

(b)

(c)

(d)
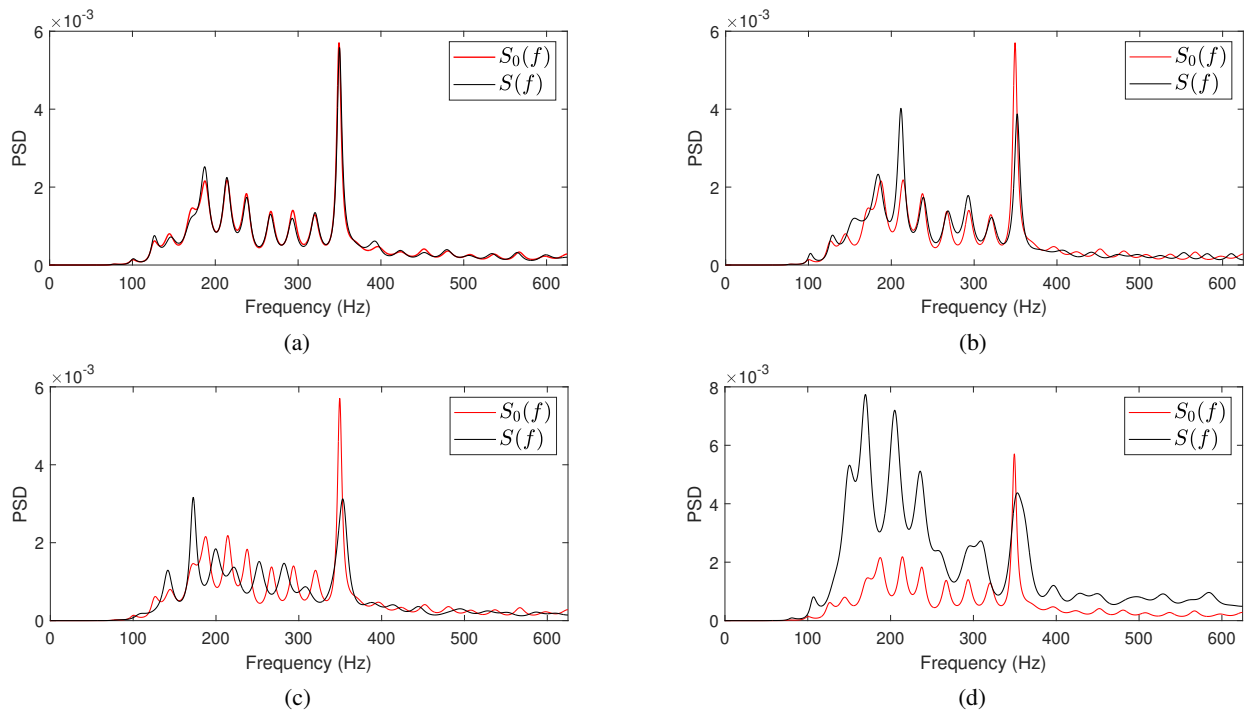
Figure 9. The reference PSD $S_0(f)$ is compared with one of the PSDs $S(f)$ obtained in the four conditions (23)–(26): (a) symmetric load (healthy state); (b) asymmetric increased load; (c) asymmetric decreased load; (d) loose symmetric load.

phases are carried out by considering different values of the length L of the sequences. Every value of the healthy indicator $SISSD$ has been obtained by considering a $db4$ wavelet and an AR model order $p = 46$. Table 2 reports, for each value of L, the mean values and the corresponding standard deviations of the $SISSD$ in the different conditions. Figure 10 reports the evolution of the healthy indicator $SISDD$ for different values of L. Only the first three configurations (23)–(25) are shown as Configuration (4) is always detected with a very large margin, as shown in Fig. (8b) and Table 2. Even though the different status of the mechanical systems can be recognized also when $L = 1250(1s)$, they start to be well

separated when $L = 2500(2s)$ and very robust thresholds can be defined for values of L equal to or greater than $5000(4s)$. The smoother behaviour of the $SISSD$ for large values of L is not surprising since AR models are identified by using more samples. It can be noted from the first column of Table 2 that the mean value of the indicator in the healthy condition tends to stabilize when L increases. The choice $L = 5000(4s)$ could be a good trade-off (see also Fig. 8); nevertheless, if the mechanism degradation takes hours or days (as expected in this kind of mechanisms) window lengths of 6 seconds or more are still quite reasonable.

The sensitivity of the proposed approach to noise is analyzed

Table 2. Mean and standard deviation of the $SISSD$ for the four Configurations (23)–(26) for different lengths L of the signal windows. Every value of the $SISSD$ has been obtained starting from a $db4$ wavelet analysis and an AR model of order $p = 46$.

	Config. (1)	Config. (2)	Config. (3)	Config. (4)
$L = 1250\,(1s)$	0.0350 ± 0.0090	0.0707 ± 0.0137	0.1301 ± 0.0234	0.9186 ± 0.1668
$L = 2500\,(2s)$	0.0119 ± 0.0030	0.0513 ± 0.0078	0.1113 ± 0.0129	0.8602 ± 0.0998
$L = 5000\,(4s)$	0.0088 ± 0.0027	0.0492 ± 0.0064	0.1055 ± 0.0103	0.8599 ± 0.1062
$L = 7500\,(6s)$	0.0073 ± 0.0026	0.0472 ± 0.0044	0.1028 ± 0.0085	0.8476 ± 0.0842
$L = 10000\,(8s)$	0.0064 ± 0.0026	0.0456 ± 0.0036	0.1007 ± 0.0079	0.8434 ± 0.0807
$L = 12500\,(10s)$	0.0058 ± 0.0017	0.0436 ± 0.0030	0.0993 ± 0.0075	0.8424 ± 0.0771
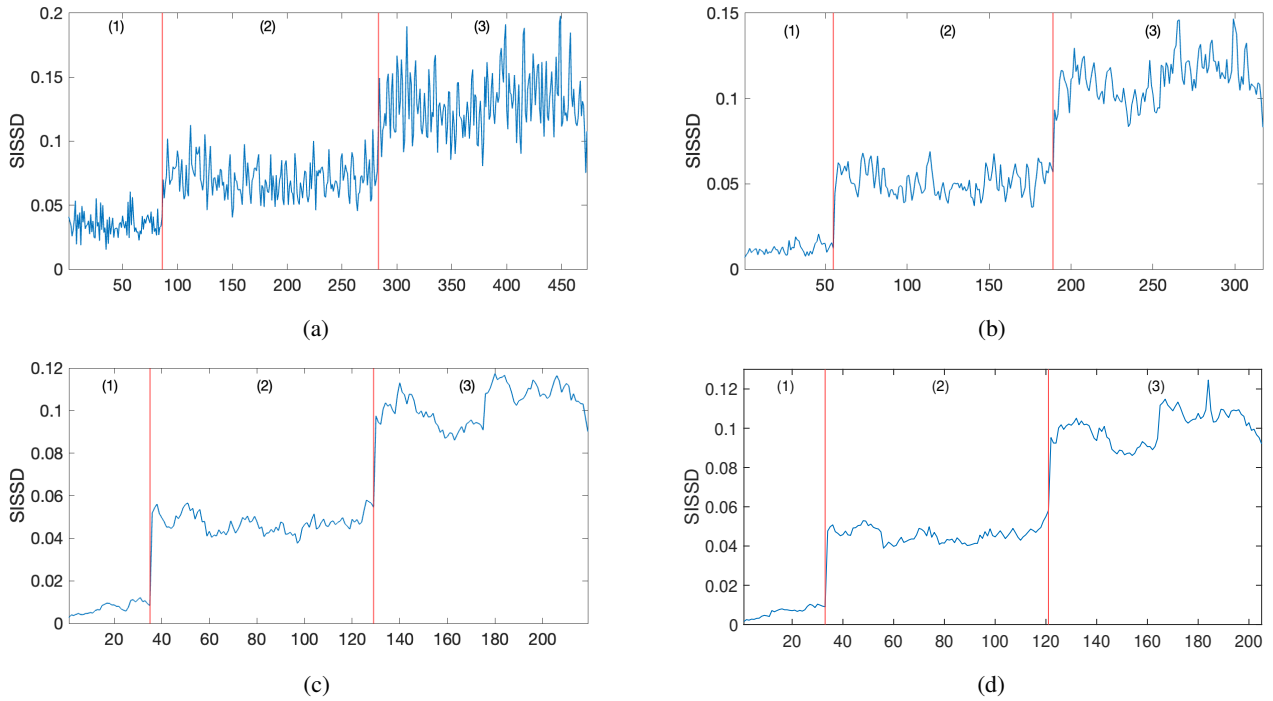
Figure 10. Evolution of the healthy indicator $SISSD$ for different values of the sequences length L: (a) $L = 1250$; (b) $L = 2500$; (c) $L = 7500$; (d) $L = 10000$. Each value of the $SISSD$ has been obtained starting from a $db4$ wavelet analysis and an AR model of order $p = 46$. Only the first three configurations are shown.

by adding white gaussian noise to the PLC torque signal (see left column of Fig. 7). The variance of the noise is selected to set a desired signal to noise ratio evaluated with respect to the informative signal extracted in healthy conditions, see Fig. 7b. The obtained results are reported in Figures 11 and 12 that refer to signal to noise ratios of 5 dB and 0 dB respectively. The procedure seems quite robust w.r.t. the presence of noise even if, by comparing Fig. 8b with Figs. 11 and 12, it can be noted that the distance between the healthy status and the faulty one decreases as the level of noise increases.

To show the robustness of the approach with respect to the wavelet parameters, both the parameters setting and online monitoring steps were repeated by exploiting the $db5$ wavelet.

The torque signals is divided into sequences of length $L = 5000$. The setting step led to the selection of $k_e = 2$ analysis levels and of an AR model order $p = 46$, as for the $db4$ wavelet. Fig. 13 reports the evolution of the healthy indicator $SISDD$ in the four configurations (23)–(26). Table 3 reports the mean values and the corresponding standard deviations of the $SISSD$ in the different conditions for various values of the sequences length L. By comparing Figs. 8 and 13 and Tables 2 and 3 it follows that the obtained results are in line with those we got by using the $db4$ wavelet.

Finally, the performance of the method is tested in a different operating conditions of the electric-cam mechanism, that is, the master runs at a constant speed $\Omega_p = 720°/s$,

(a)

(b)
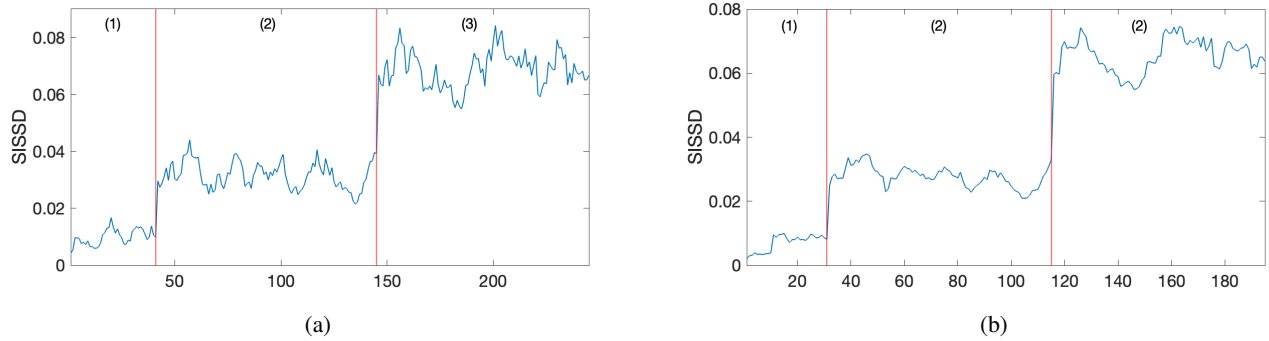
Figure 11. Evolution of the healthy indicator $SISSD$ in the different conditions (23)–(25) in the presence of noise (SNR=5 dB): (a) $L = 5000$; (b) $L = 10000$. Each value of the $SISSD$ has been obtained starting from a $db4$ wavelet analysis and an AR model of order $p = 46$.

(a)

(b)
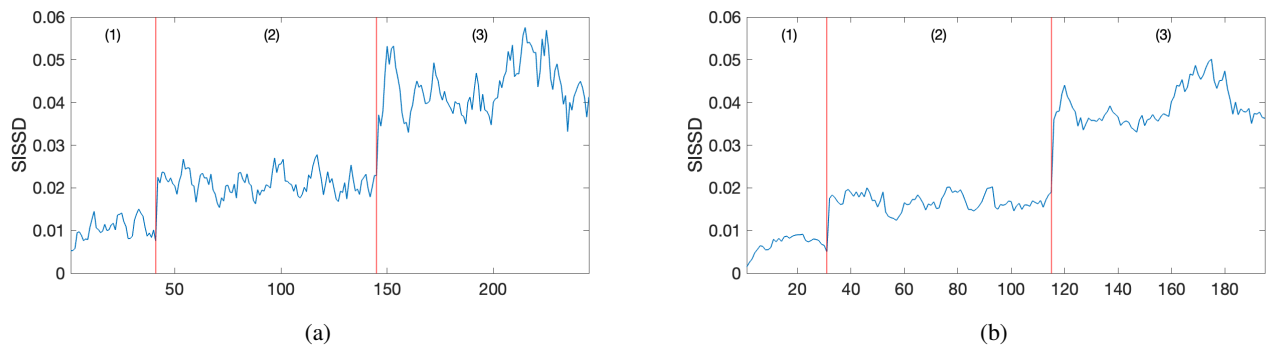
Figure 12. Evolution of the healthy indicator $SISSD$ in the different conditions (23)–(25) in the presence of noise (SNR=0 dB): (a) $L = 5000$; (b) $L = 10000$. Each value of the $SISSD$ has been obtained starting from a $db4$ wavelet analysis and an AR model of order $p = 46$.

(a)

(b)
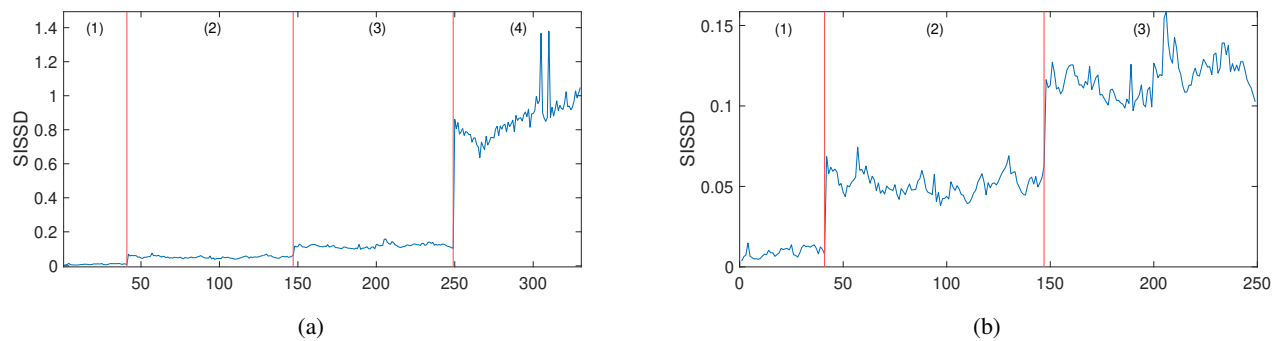
Figure 13. Evolution of the healthy indicator $SISSD$ in the different conditions (23)–(26). Each value of the $SISSD$ has been obtained starting from a sequence of length $L = 5000$, a $db5$ wavelet analysis and an AR model of order $p = 46$. (a) all configurations are considered; (b) zoom of (a) to clearly show the behaviour of the $SISSD$ in the first three conditions.

lower than the speed of the first experiments $\Omega_p = 1080°/s$. Both the parameters setting and the online monitoring phases are carried out by using a $db4$ wavelet with $k_e = 2$ analysis levels and AR models of order $p = 46$. This condition is more challenging than the previous one as the number of window samples L required to get a successful detection has to be increased. Figure 14 reports the evolution of the

healthy indicator $SISDD$ in the three configurations (23)–(25) for $L = 7500$ and $L = 12500$. In this case, acceptable results are obtained by considering at least $L = 7500(6s)$ and more robust detection thresholds can be defined when $L = 12500(10s)$. As already mentioned, a window length of $10s$ is quite reasonable for this kind of systems.

14

Table 3. Mean and standard deviation of the $SISSD$ for the four Configurations (23)–(26) for different lengths L of the signal windows. Every value of the $SISSD$ has been obtained starting from a $db5$ wavelet analysis and an AR model of order $p = 46$.

	Config. (1)	Config. (2)	Config. (3)	Config. (4)
$L = 1250\,(1s)$	0.334 ± 0.0086	0.0703 ± 0.141	0.1403 ± 0.0208	0.9093 ± 0.1431
$L = 2500\,(2s)$	0.0123 ± 0.0034	0.0540 ± 0.0085	0.1229 ± 0.0140	0.8675 ± 0.1170
$L = 5000\,(4s)$	0.0092 ± 0.0030	0.0514 ± 0.0068	0.1175 ± 0.00118	0.8621 ± 0.1213
$L = 7500\,(6s)$	0.0073 ± 0.0021	0.0477 ± 0.0049	0.1145 ± 0.0091	0.8327 ± 0.0824
$L = 10000\,(8s)$	0.0065 ± 0.0027	0.0478 ± 0.0043	0.1123 ± 0.0090	0.8323 ± 0.0777
$L = 12500\,(10s)$	0.0060 ± 0.0017	0.0457 ± 0.0037	0.1125 ± 0.0089	0.8353 ± 0.0768

(a)

(b)
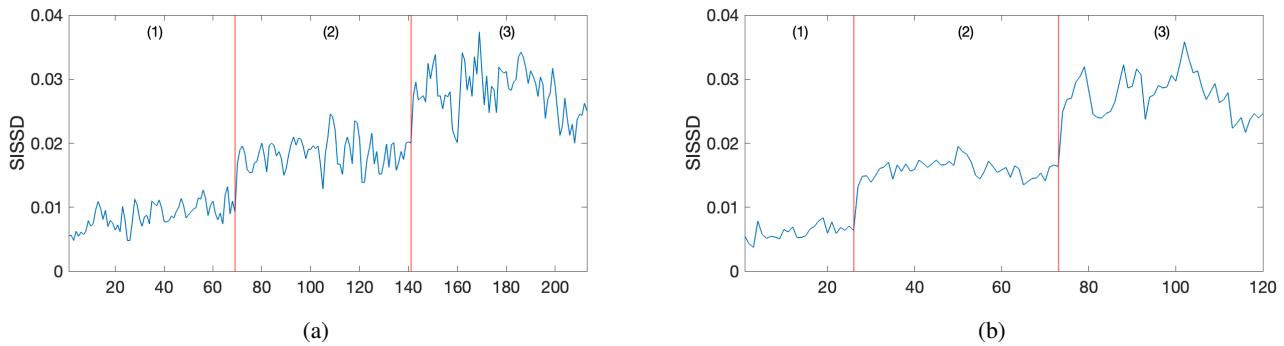
Figure 14. Evolution of the healthy indicator $SISSD$ in the different conditions (23)–(25) for a lower speed of master ($720°/s$ instead of $1080°/s$): (a) $L = 7500(6s)$; (b) $L = 12500(10s)$. Each value of the $SISSD$ has been obtained starting from a $db4$ wavelet analysis and an AR model of order $p = 46$.

6. CONCLUSION

This paper describes a new procedure for the condition monitoring of electric-cam mechanisms in PLC controlled machines. The proposed data-driven approach is based on the motor absorbed torqued provided by the PLC. The torque signal is modelled as the sum between the nominal (ideal) torque and an additive contribution containing information on the state of health of the mechanism. In order to get the informative part of the measured torque, a new combination of wavelets analysis and autoregressive model identification is employed. The whole procedure is non invasive and allows real-time analysis since it is based on efficient filtering and estimation techniques performed on a signal readily available in industrial computers complying with the PLCopen standard. The results obtained on real data collected in a laboratory setup demonstrate the effectiveness of the proposed method in both detecting and classifying faults.

REFERENCES

Barbieri, M., Bosso, A., Conficoni, C., Diversi, R., Sartini, M., & Tilli, A. (2018). An onboard model-of-signals approach for condition monitoring in automatic machines. In *Enterprise interoperability: Smart services and business impact of enterprise interoperability* (pp. 263–269). Wiley – ISTE.

Barbieri, M., Diversi, R., & Tilli, A. (2019). Condition monitoring of ball bearings using estimated AR models as logistic regression features. In *2019 18th European Control Conference (ECC 2019)* (pp. 3904–3909).

Barbieri, M., Diversi, R., & Tilli, A. (2020). Condition monitoring of electric-cam mechanisms based on model-of-signals of the drive current higher-order differences. *IFAC-PapersOnLine*, *53*(2), 802-807.

Barbieri, M., Nguyen, K. T. P., Diversi, R., Medjaher, K., & Tilli, A. (2021). RUL prediction for automatic machines: a mixed edge-cloud solution based on model-of-signals and particle filtering techniques. *Journal of Intelligent Manufacturing*, *32*, 1421–1440.

Basseville, M. (1988). Detecting changes in signals and systems—a survey. *Automatica*, *24*(3), 309-326.

Biagiotti, L., & Melchiorri, C. (2008). *Trajectory planning for automatic machines and robots*. Springer Science & Business Media.

Box, G. E., Jenkins, G. M., Reinsel, G. C., & Ljung, G. M. (2015). *Time series analysis: forecasting and control*. John Wiley & Sons.

Cerrada, M., Sánchez, R.-V., Li, C., Pacheco, F., Cabrera, D.,

de Oliveira, J. V., & Vásquez, R. E. (2018). A review on data-driven fault severity assessment in rolling bearings. *Mechanical Systems and Signal Processing*, *99*, 169–196.

Chai, N., Yang, M., Ni, Q., & Xu, D. (2018). Gear fault diagnosis based on dual parameter optimized resonance-based sparse signal decomposition of motor current. *IEEE Transactions on Industry Applications*, *54*(4), 3782-3792.

Daubechies, I. (1992). *Ten lectures on wavelets*. SIAM.

Foundation, P. (1992). *Plcopen foundation*. Retrieved from `https://plcopen.org/technical-activities/motion-control` (Accessed: 2023-11-01)

Gouriveau, R., Medjaher, K., & Zerhouni, N. (2016). *From prognostics and health systems management to predictive maintenance 1: Monitoring and prognostics*. John Wiley & Sons.

Grivel, E., Diversi, R., & Merchan, F. (2021). Kullback-Leibler and Rényi divergence rate for Gaussian stationary ARMA processes comparison. *Digital Signal Processing*, *116*, 103089.

Isermann, R. (2005). Model-based fault-detection and diagnosis–status and applications. *Annual Reviews in control*, *29*(1), 71–85.

Isermann, R. (2006). *Fault-diagnosis systems: an introduction from fault detection to fault tolerance*. Springer Science & Business Media.

Jardine, A. K., Lin, D., & Banjevic, D. (2006). A review on machinery diagnostics and prognostics implementing condition-based maintenance. *Mechanical systems and signal processing*, *20*(7), 1483–1510.

Kar, C., & Mohanty, A. (2006). Monitoring gear vibrations through motor current signature analysis and wavelet transform. *Mechanical Systems and Signal Processing*, *20*(1), 158-187.

Lee, J., Wu, F., Zhao, W., Ghaffari, M., Liao, L., & Siegel, D. (2014). Prognostics and health management design for rotary machinery systems – Reviews, methodology and applications. *Mechanical systems and signal processing*, *42*(1-2), 314–334.

Ljung, L. (1999). *System identification: theory for the user*. Prentice-hall.

Mallat, S. (1989). A theory for multiresolution signal decomposition: the wavelet representation. *IEEE Transactions on Pattern Analysis and Machine Intelligence*, *11*(7), 674-693.

Nandi, S., Toliyat, H. A., & Li, X. (2005). Condition monitoring and fault diagnosis of electrical motors -— A review. *IEEE transactions on energy conversion*, *20*(4), 719–729.

Peng, Z., & Chu, F. (2004). Application of the wavelet transform in machine condition monitoring and fault diagnostics: A review with bibliography. *Mechanical Systems and Signal Processing*, *18*(2), 199 – 221.

Pincus, S. (1995). Approximate entropy (ApEn) as a complexity measure. *Chaos An Interdisciplinary Journal of Nonlinear Science*, *5*(1), 110-117.

Qi, R., Zhang, J., & Spencer, K. (2023). A review on data-driven condition monitoring of industrial equipment. *Algorithms*, *16*(1).

Singh, S., & Kumar, N. (2017). Detection of bearing faults in mechanical systems using stator current monitoring. *IEEE Transactions on Industrial Informatics*, *13*(3), 1341-1349.

Söderström, T., & Stoica, P. (1989). *System identification*. Prentice Hall.

Soualhi, A., Hawwari, Y., Medjaher, K., Clerc, G., Hubert, R., & Guillet, F. (2017). Prognostics and health management for maintenance practitioners - review, implementation and tools evaluation. *International Journal of Prognostics and Health Management*, *8*(3).

Soualhi, A., Hawwari, Y., Medjaher, K., Clerc, G., Hubert, R., & Guillet, F. (2018). PHM survey: Implementation of signal processing methods for monitoring bearings and gearboxes. *International Journal of Prognostics and Health Management*, *9*(2).

Strang, G., & Nguyen, T. (1996). *Wavelets and filter banks*. Wellesley-Cambridge Press.

Wei, B., & Gibson, J. (2000). Comparison of distance measures in discrete spectral modeling. In *Proc. of the 9th Digital Signal Processing Workshop*.

Yan, R., Gao, R. X., & Chen, X. (2014). Wavelets for fault diagnosis of rotary machines: A review with applications. *Signal Processing*, *96*, 1-15.